PNAS RESEARCH ARTICLE | ENVIRONMENTAL SCIENCES

Cooperative mixing through hydrodynamic interactions in *Stylonychia lemnae*

Régis Turuban[a,b,1], Giovanni Noselli[b], Alfred Beran[c], and Antonio DeSimone[a,b,1]

Affiliations are included on p. 11.

Edited by Howard Stone, Princeton University, Princeton, NJ; received January 28, 2025; accepted July 27, 2025

Aquatic microorganisms typically inhabit a heterogeneous resource landscape, composed of localized and transient patches. To effectively exploit these resources, they have evolved a wide range of feeding strategies that combine chemotactic motility with active feeding flows. However, there is a notable lack of experimental studies that examine how these active flows shape resource fields to optimize feeding. In particular, the suspected cooperative hydrodynamics provided by groups of cells remains largely unexplored due to the difficulties in visualizing these dynamic three-dimensional flows. Here, we experimentally investigate how *Stylonychia lemnae* ciliates form feeding clusters of independent cells around food patches. Individual feeding flows interact hydrodynamically to create a chaotic collective flow at the population scale. Using a combination of experimental and numerical techniques, we measure and predict the entire collective flow, enabling us to assess its remarkable mixing and dispersion properties. We show that the active spreading of the food patch accelerates its detection by starving cells. As many fitness advantages provided by collective flows can be envisioned, we propose that this feeding cluster represents a form of intraspecific by-product cooperative behavior.

Stylonychia | intraspecific cooperation | feeding efficiency | chaotic mixing

Significance

To optimize foraging in a viscous environment, aquatic microorganisms use chemotactic motility or generate feeding flows. Some form colonies, possibly improving prey uptake through hydrodynamic interactions. In this study, we investigate how a group of *Stylonychia lemnae* ciliates interacts with food patches. As cells aggregate around a patch, they generate a chaotic collective flow that redistributes food within the population. We measure and predict the flow's properties, showing that it enlarges the food patch faster than individual swimming would, thereby accelerating food detection by starving cells. We interpret the behavior of the cluster as cooperative in terms of hydrodynamic interactions and emphasize the importance of accounting for the stochastic motions of individual cells that drive the chaotic flow.

Survival for aquatic microorganisms is about encountering: maximizing interactions with prey or nutrients for feeding and minimizing encounters with predators (1). Often, interactions are mediated by the chemical signals constantly released by microorganisms, whether they wish it or not. To best exploit patchy resource fields (2–5) in a viscous world, microorganisms have evolved the ability to navigate concentration gradients toward the source (chemotaxis) and/or actively generate flows powerful enough to shape concentration gradients directly. Examples of such actively generated flows include the currents around the organism's body as it swims (6–8), feeding flows produced by microorganisms either anchored to a solid substrate (9–13), tethered by gravity (14), or bonded together within a colony (15–18), as well as hydrodynamic waves triggered by rapid body contractions (19) or the long-range coherent flows produced by active suspension of pushers (20, 21). Faced with this diversity of cell organizations and their associated active flows, scientists have long wondered which fluid kinematics would lead to optimal feeding rates/nutrient uptake, and under which specific conditions.

Particularly well-suited to tackle this problem are the organisms exhibiting different morphotypes, ranging from unicellular to undifferentiated multicellular colonies. For example, refs. 15 and 22 have shown that *volvox* colonies—spherical colonies made up of thousands of Chlamydomonas cells bonded together—balance their expanding metabolic needs as their radius R grows by generating flows of increasing magnitude that steepen concentration gradients and thus ultimately enhance the diffusion flux, scaling just as the expanding surface $Q \sim R^2$. Other research by ref. 16 estimates that cooperative hydrodynamics within choanoflagellate colonies (which are attached together in the fluid bulk) increase the fresh fluid supply per cell compared to freely swimming single cells. However, another study by ref. 17 presents a contrasting view, predicting that choanoflagellate colonies are less advantageous in terms of feeding flux compared to single anchored cells, which in turn are less advantageous than freely swimming cells. Although the prediction that freely swimming provides the highest feeding rate is consistent with the results of ref. 23, it contradicts experimental findings indicating that cells tend to promote swimming over anchoring and feeding when deprived of food (24). Moreover, the claim that colonies are the least advantageous organization is challenged by the findings of ref. 25, which showed that in some choanoflagellate species, colony formation is triggered by sensing chemicals produced by their prey bacteria, even at very

Author contributions: R.T. designed research; R.T. performed research; R.T., G.N., and A.D. analyzed data; R.T. and G.N. designed experiments; A.B. grew cells and shared expertise on biology; A.D. supervised research, acquired funding; and R.T., G.N., A.B., and A.D. wrote the paper.

The authors declare no competing interest.

This article is a PNAS Direct Submission.

Copyright © 2025 the Author(s). Published by PNAS. This article is distributed under Creative Commons Attribution-NonCommercial-NoDerivatives License 4.0 (CC BY-NC-ND).

[1]To whom correspondence may be addressed. Email: rturuban@sissa.it or desimone@sissa.it.

This article contains supporting information online at https://www.pnas.org/lookup/suppl/doi:10.1073/pnas.2500588122/-/DCSupplemental.

Published September 8, 2025.

Downloaded from https://www.pnas.org by Scuola Internazionale Superiore di Studi Avanzati SISSA on December 1, 2025 from IP address 147.122.98.209.

low concentrations. Clearly, the systematic feeding advantages conferred by diverse fluid kinematics—especially in the case of colonies—are still poorly understood.

To reconcile predictions with observations, a better understanding of the dynamic interaction between organisms and the nutrient/prey field is required. So far, the vast majority of studies have based their numerical estimations of feeding rates on strong simplifications: a cell generating a steady active flow, in a still ambient fluid, and immersed in a uniform resource field. The latter two conditions hold true only for $\mathrm{Pe}_{\mathrm{ambient}} < 1$, yet many organisms operate in the $\mathrm{Pe}_{\mathrm{ambient}} > 1$ regime (26) (where $\mathrm{Pe}_{\mathrm{ambient}} = v_{\mathrm{ambient}} L/D$ is the Péclet number relative to the ambient velocity field v_{ambient}, L the characteristic flow size, and D the diffusion coefficient). Regarding the first condition, unsteadiness is rarely discussed, although (27, 28) have demonstrated that the simple case of two nearby sessile cells alternating feeding currents can drastically enhance feeding by introducing Lagrangian chaos. In fact, experimental observations of microorganisms interacting with a resource field in the large Pe regime reveal much more dynamic behavior, as illustrated by the striking collective behavior exhibited by both the bacterium *Thiovulum majus* and the ciliate *Uronemella* (29–31). In this case, the authors suggest that the cell's oxygen consumption results from the highly dynamic interplay between three components: i) their locomotion behavior, which depends on gradients of both O_2 and population density; ii) the macroscopic active flow produced by the community, controlled by local population density; and iii) the O_2 concentration field advected by the macroscopic flow, and consumed by the cells. Thus, these studies underscore the need to revisit the feeding problem in a patchy food environment by taking into account this complex coupling. This requires experimental measurements of the evolving 3D active flow, which, to our knowledge, have not yet been performed.

Here, we propose to experimentally investigate the feeding behavior of *Stylonychia lemnae* (32) evolving in a patchy food environment. *S. lemnae* is a 200 μm long freshwater ciliate belonging to Spirotrichea, a class of ciliates widely distributed across diverse ecosystems, including freshwater, saltwater, soils, and activated sludge (33). *S. lemnae* can either swim or attach itself to interfaces and crawl. Being anchored to solid boundary allows the cell to exert a net force on the fluid using its adoral zone of membranelles (AZM; see Fig. 1 *A* and *B* and Movies S1 and S2), directing the fluid toward its buccal apparatus. Our research reveals that *S. lemnae* exhibits a collective feeding behavior that closely resembles that of *T. majus* and *Uronemella*, characterized by individual chemosensory locomotion to locate and remain near food patches, resulting in cell clustering around these patches. Next, multiple hydrodynamic interactions lead to flow at the population scale. However, unlike *volvox*, choanoflagellates colonies or the veils of *Uronemella*, where cells are bound together, the cells in *S. lemnae* feeding clusters remain strictly independent. This leads to an important question: Can such a loosely organized group of cells, lacking physical connections, exhibit cooperative behavior through hydrodynamic interactions? To this end, we experimentally characterize both locomotion behavior and the full 3D unsteady flow generated by a feeding cluster of *S. lemnae*. We numerically quantify the dispersion and mixing kinematics of the collective flow. By combining these two elements within the lamellar approach (34, 35), we are able to predict the rate at which any patchy resource field is distributed and homogenized within the feeding cluster.

1. Sensing Food Triggers a Change of Locomotion Behavior in *S.lemnae*

In laboratory conditions, when starving, *S. lemnae* typically wanders on the floor of a Petri dish looking for food, as illustrated in Fig. 1*D*. Thanks to its cirri, it crawls in wide leftward arcs over distances up to several millimeters, with an average speed of $\langle v_c \rangle \approx 790\,\mu\mathrm{m/s}$ ($\pm\sigma_{v_c} \approx 670\,\mu\mathrm{m/s}$), peaking at $v_c \sim 7{,}000\,\mu\mathrm{m/s}$ (i.e. $35L_c$/s, with $L_c \approx 200\,\mu\mathrm{m}$ the average cell length). The leftward arcs are interspersed with sudden stops ($v_c = 0$), which can last from a few tens of milliseconds to a few tens of seconds. Then, either the cell resumes its movement forward, or it performs abrupt moves called Side-Stepping Reactions (SSRs), typically observed in Spirotrich species such as *S. mytilus* or *Euplotes* (36–38). These movements involve two steps: bouncing backward, then rotating clockwise by a varying angle $\Delta\theta$. An example of a cell performing three successive SSR moves can be seen in Fig. 1*C*, resulting in that particular case in a complete revolution (Movie S3).

We noticed a drastic change in locomotion behavior whenever *S. lemnae* senses food. To quantify it, we conducted the following experiment. In the first step, the positions of starving cells are tracked for 5 min. In the second step, we inject food (either yeast or *Chlorogonium* algae) and gently stir it by hand until the food concentration is homogeneous inside the whole Petri dish. Another sequence of images is then taken for 5 min. Cell trajectories are reconstructed using particle tracking velocimetry (PTV) and Lagrangian velocities v_c extracted from displacements between successive images (*SI Appendix*, section 2A for details). A first qualitative difference of locomotion patterns can be inferred from the comparison between Fig. 1 *D* and *E* (Movie S4). Clearly, cells deprived of food travel much farther, whereas cells in the presence of food shorten their crawling segments and make longer stops. With reduced travel, SSR movements mostly result in rotation around a point, with minimal drift. At the macroscopic scale, this behavioral change is quantified by the mean squared displacement (MSD), defined as the variance of cell displacements $\sigma_{\boldsymbol{x}}^2 = \langle |\boldsymbol{x}(t) - \boldsymbol{x}(0)|^2 \rangle$, with $\langle \ldots \rangle$ the ensemble average over all trajectories i, after checking that cell spreading is isotropic, i.e. $\langle \boldsymbol{v_c} \rangle = 0$. The MSDs for both cases are compared in Fig. 1*G*. The MSD for the no-food case well captures the early-time ballistic regime $\sigma_{\boldsymbol{x}}^2 \sim t^2$. After a coherence time, the MSDs shift to a diffusive regime $\sigma_{\boldsymbol{x}}^2 \sim t$, but this regime is soon limited by the finite imaging area (cells exiting the field of view). To overcome this limitation and get the asymptotic scaling, we compute the MSD from the velocity autocorrelation function (VAF) (*SI Appendix*, section 2B), which are related through the expression $\sigma_{\boldsymbol{x}}^2 = 2\int_0^t d\tau (t-\tau) C(\tau)$, with $C(\tau) = \langle \boldsymbol{v_c}(\tau) \cdot \boldsymbol{v_c}(0) \rangle$, whose graphs are displayed in Fig. 1*F*, as a function of the time lag $\tau = t' - t''$. The new MSD graphs are superimposed onto the previous MSDs in the same Fig. 1*G*, and reveal that both MSDs reach a Fickian regime $4Dt$, though with a dispersion coefficient D that varies with ambient conditions. These dispersion coefficients are computed via the Green–Kubo relation $D = \frac{1}{2}\int_0^\infty d\tau \langle \boldsymbol{v_c}(\tau) \cdot \boldsymbol{v_c}(0) \rangle$. We get $D_{\mathrm{NF}} = 4.3 \times 10^{-7}\ \mathrm{m^2/s}$ (no-food) and $D_{\mathrm{WF}} = 4.5 \times 10^{-8}\ \mathrm{m^2/s}$ (with-food), indicating that cells span space $D_{\mathrm{NF}}/D_{\mathrm{WF}} \approx 10$ times slower when food is present. This drop is due in part to the slightly faster decay of $C(\tau)/C(0)$ as shown in Fig. 1*F*, but mostly from an overall reduction in locomotion speed v_c through the ratio $C(0)_{\mathrm{NF}}/C(0)_{\mathrm{WF}} = \langle \boldsymbol{v_c}^2 \rangle_{\mathrm{NF}} / \langle \boldsymbol{v_c}^2 \rangle_{\mathrm{WF}} \approx 4.7$. This is confirmed by the velocity distribution $P(v_c)$ shown in

Downloaded from https://www.pnas.org by Scuola Internazionale Superiore di Studi Avanzati SISSA on December 1, 2025 from IP address 147.122.98.209.

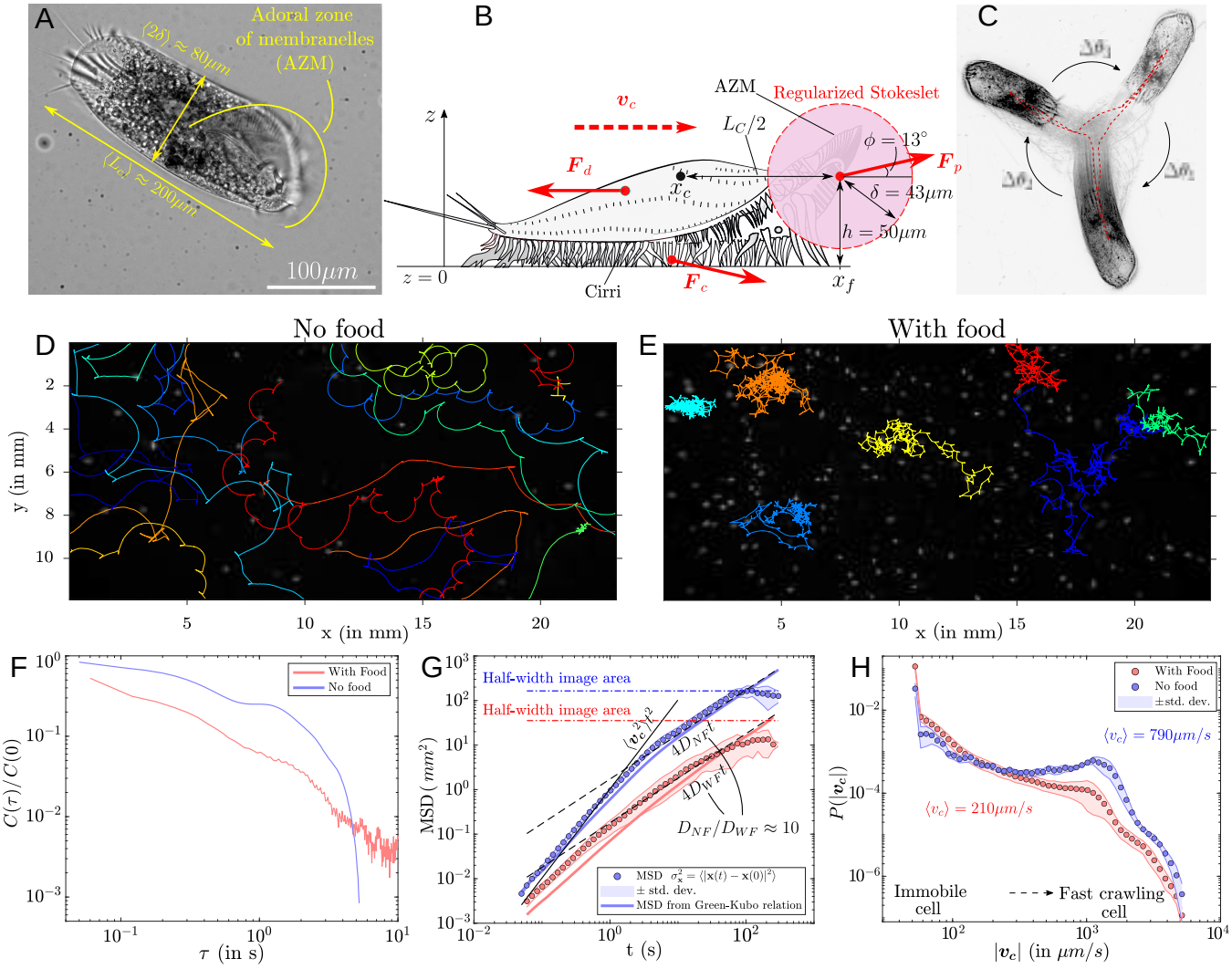

Fig. 1. *S. lemnae*'s locomotion behavior. (*A*) Microscopy image of a *S. lemnae* cell viewed from below. (*B*) Schematic lateral view (adapted from the *Stylonychia* Wikipedia webpage), and the balance of forces acting on the cell body during crawling locomotion at speed v_c. (*C*) A *S. lemnae* cell performing a series of three Side-Stepping Reactions (SSRs). The cell's trajectory is displayed as a red dashed line. (*D*) Trajectories $\boldsymbol{x}_i(t)$ followed by starving *S. lemnae* as they crawl on the bottom of their Petri dish culture. (*E*) Trajectories followed by the same cells ∼1 to 2 min after the injection and manual mixing of food. These trajectories are selected so that they do not overlap. (*F*) Normalized autocorrelation function of the crawling velocities $\boldsymbol{v_c}$ (VAFs) for the two distinct ambient conditions: no food (in blue) and with food (in red). (*G*) Mean square displacement (MSD) calculated either from the variance of cell displacements (dots), or from the Green–Kubo relation (continuous lines), computed from the VAFs in panel (*F*). Same color code as before. Error bars (shaded area) indicate the SD across seven different datasets. The continuous black line represents ballistic transport at early times, scaling as $\sigma_{\boldsymbol{x}}^2 \sim \langle \boldsymbol{v_c}^2 \rangle t^2$, for the no-food case. The black dashed lines represent the asymptotic Fickian regime $\sigma_{\boldsymbol{x}}^2 \sim 4Dt$ reached in both cases, with different dispersion coefficient D_{NF} (no-food) and D_{WF} (with-food). The colored dashed lines indicate the image boundary beyond which cells are out of view. (*H*) Probability density function of cell speed $P(|\boldsymbol{v_c}|)$ under the two ambient conditions. The minimum measurable velocity with our setup is $v_c^{\min} = 50\,\mu$m/s, below which the cell is considered immobile.

Fig. 1*H*, which reveals that food injection triggers a massive drop in high-speed events, with a fivefold drop in mean speed $\langle v_c \rangle$. Thus, cells switch between two locomotion modes depending on food availability, primarily by modulating v_c–a well-known chemotactic strategy to remain in favorable areas (39).

2. Formation of a Cluster of Feeding Cells Around a Food Injection Site and Collective Fluid Mixing

To mimic the patchy food environment in which many organisms live (2, 3), we conduct a similar experiment, with the difference that the food is now injected within a confined region (*SI Appendix*, section 3). About $M_{\mathrm{yeast}} = 0.25 \pm 0.10$ mg of yeast (i.e. almost three orders of magnitude larger than the amount a single cell can consume, assuming it can ingest up to 25% of its own volume) is injected at position $\mathbf{x}_{\mathrm{inj}}$ among starving crawling cells (see Fig. 2 *A*, (*i*) and *SI Appendix*, Fig. S2, extracted from Movies S5 and S6, respectively). The food blob is originally $s_0 \approx 0.5$ mm $= 2.5L_c$ in diameter. Before injection, cells exhibit persistent long traveling paths that frequently reach values up to $20L_c$ (with peaks of $50L_c$), when integrated over a period of 5 s. Immediately after injection (Fig. 2 *A*, (*i*), $t = 5$ s), only cells that come into contact with the injected food blob drastically reduce their traveled path but, over time, even distant cells restrict their amplitude of motion (Fig. 2 *A*, (*ii*), $t = 280$ s). The transition toward shortened movement over time is shown in Fig. 2*B*. After $t = 400$ s, most cells no longer travel, even those far from the injection point (up to 1 cm, i.e. $20s_0$): A feeding cell cluster has formed. The phenomenon is all the more intriguing given that yeast diffuses very slowly, with $D_{\mathrm{yeast}} \approx 10^{-11}$ m^2/s as given by the Stokes–Einstein equation. Importantly, cluster

Downloaded from https://www.pnas.org by Scuola Internazionale Superiore di Studi Avanzati SISSA on December 1, 2025 from IP address 147.122.98.209.

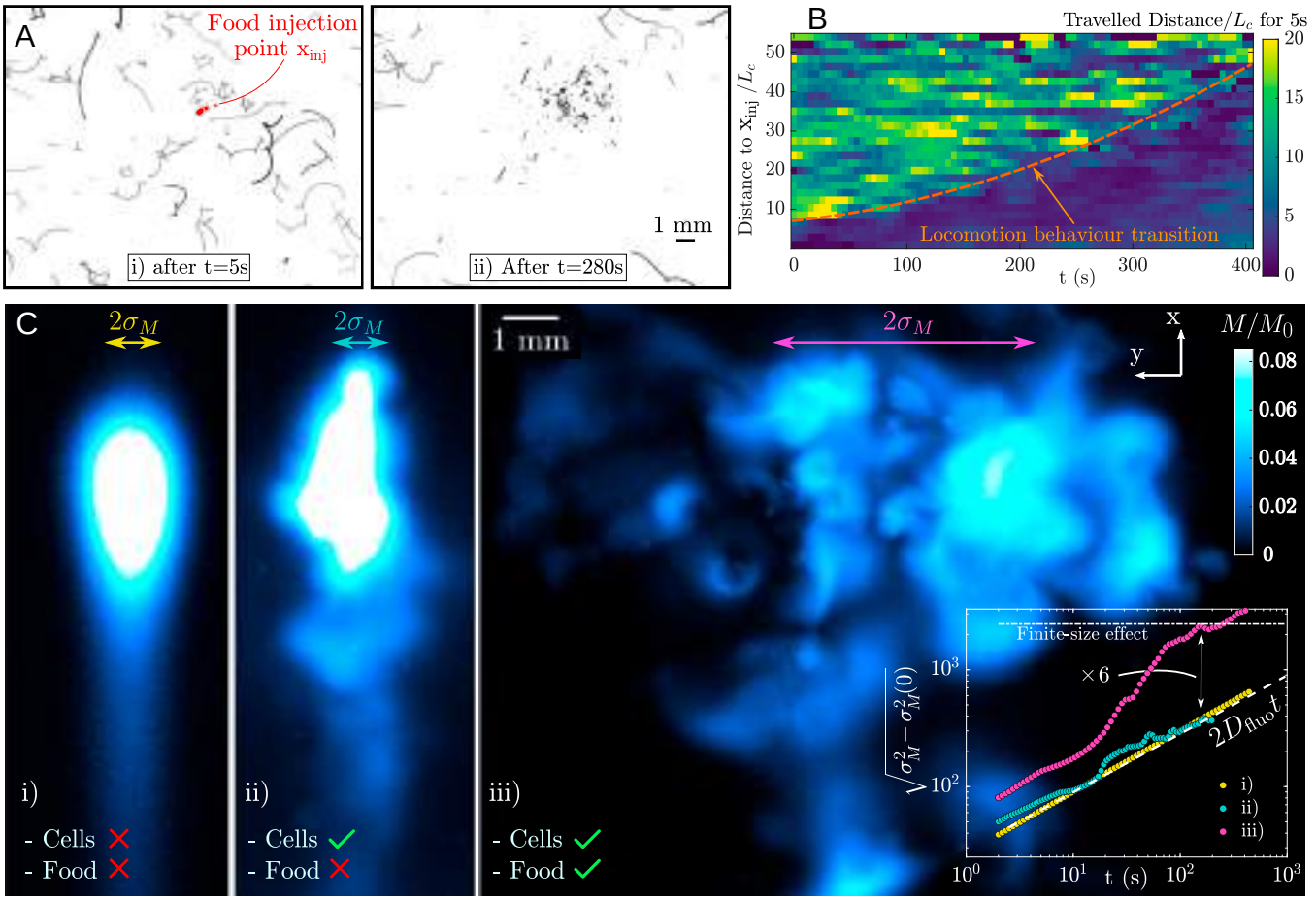

Fig. 2. Collective flow by a feeding cell cluster. (*A*) Trajectories of a few *S. lemnae* integrated over 5 s, from i) $t = 5$ s and ii) $t = 280$ s after the local injection of yeast, at position x_{inj}. (*B*) Temporal evolution of the distance traveled by different *S. lemnae* over 5 s, depending on their initial distance from the food injection point x_{inj}. The statistical analysis is based on ≈640 trajectories from one experiment. The orange continuous line shows the transition between the two locomotion behavior triggered further and further away from the food injection point as time progresses. Initially, about 50 cells are visible on the images, progressively increasing to reach up to 100 cells, 400 s after the injection. (*C*) Imaging of a fluorescein blob injected in the observation chamber either i) in the absence of *S. lemnae* cells, or ii) injected among cells, or iii) mixed with yeast prior to injection among cells. These snapshots were taken at $t = 174$ s after the injection of the dye blob. Fluorescence intensity levels $I(x, y)$ are converted to mass levels $M(x, y)$ normalized by the initial mass M_0. *Inset*: Temporal evolution of the spatial variance of fluorescein mass in the *y*-direction, $\sqrt{\sigma_M^2 - \sigma_M^2(0)}$, for the 3 cases. The yellow, cyan, and purple arrows superimposed on the images depict the width $2\sigma_M$ of the Gaussian function that would fit the *y*-profile of the three mass fields.

formation is consistently reproducible, regardless of the cells' food vacuole fullness. Indeed, although at the high initial food concentration the cells may become fully fed in just a few seconds and stop ingesting food (Movie S7), this does not affect their locomotion behavior, which depends primarily on the detected food concentration (*SI Appendix*, section 4).

To understand how food detection by cells occurs at an increasing distance from the injection point, and to reveal any potential flow, we perform a passive solute tracer experiment by injecting a mixture of yeast with fluorescein-dyed water among a group of *S. lemnae*. To do so, a few tens of cells are transferred to an observation chamber consisting of two parallel glass plates separated by a 3 mm gap, large enough to avoid confinement effects (40). The dyed mixture is injected using a syringe, and imaging begins promptly after its withdrawal. The evolving fluorescein field is imaged using LED-Induced Fluorescence (LEDLIF), where the fluorescence intensity field $I(x, y)$ in the raw image is converted to mass $M(x, y)$ of fluorescein accumulated in the z-column above each pixel (x, y), via the linear relation $M(x, y) \propto I(x, y)$ (see *SI Appendix*, section 5 for the full procedure).

We compare tracer transport in the presence of food to two control experiments: i) pure diffusion, with fluorescein injected in the observation chamber without cells, and ii) fluorescein injected among cells but without yeast. Fig 2*C* shows images of the dye blobs from each of the three experiments, taken 3 min after injection (Movie S8). In the cell-only case ii), the dye blob undergoes some local and intermittent stirring, but its final shape is quite similar to that of the purely diffusive case i). By contrast, Fig 2 *C*, (*iii*) reveals how *S. lemnae* cells, in the presence of food, actively generate a large-scale chaotic flow that, in turn, dramatically reshapes and spreads fluorescein throughout the observation chamber. The steep mass gradients consistently observed throughout the experiment indicate an active Péclet number higher than unity $\mathrm{Pe}_{\mathrm{active}} = vd/D_{\mathrm{fluo}} > 1$, with $D_{\mathrm{fluo}} \approx 4.10^{-10}\,\mathrm{m}^2/\mathrm{s}$ the theoretical molecular diffusion coefficient of fluorescein (i.e. only five times lower than the oxygen diffusion coefficient $D_{O_2} \approx 2.10^{-9}\,\mathrm{m}^2/\mathrm{s}$). A more quantitative comparison between the tracer experiments can be made by measuring the spatial variance of the mass field in the y direction: $\sigma_M^2 = \Sigma_i (y_i - \mu)^2 M(x_i, y_i)/\Sigma_i M(x_i, y_i)$, with $\mu = \Sigma_i y_i M(x_i, y_i)/\Sigma_i M(x_i, y_i)$ the mass-weighted mean position

Downloaded from https://www.pnas.org by Scuola Internazionale Superiore di Studi Avanzati SISSA on December 1, 2025 from IP address 147.122.98.209.